

# ASTRA: A Scene-aware TRAnsformer-based model for trajectory prediction

Izzeddin Teeti\*    Aniket Thomas†    Munish Monga†    Sachin Kumar†  
Uddeshya Singh†    Andrew Bradley\*    Biplab Banerjee†    Fabio Cuzzolin\*  
iteeti@brookes.ac.uk,

January 20, 2025

## Abstract

We present ASTRA (A Scene-aware TRAnsformer-based model for trajectory prediction), a light-weight pedestrian trajectory forecasting model that integrates the scene context, spatial dynamics, social inter-agent interactions and temporal progressions for precise forecasting. We utilised a U-Net-based feature extractor, via its latent vector representation, to capture scene representations and a graph-aware transformer encoder for capturing social interactions. These components are integrated to learn an agent-scene aware embedding, enabling the model to learn spatial dynamics and forecast the future trajectory of pedestrians. The model is designed to produce both deterministic and stochastic outcomes, with the stochastic predictions being generated by incorporating a Conditional Variational Auto-Encoder (CVAE). ASTRA also proposes a simple yet effective weighted penalty loss function, which helps to yield predictions that outperform a wide array of state-of-the-art deterministic and generative models. ASTRA demonstrates an average improvement of 27%/10% in deterministic/stochastic settings on the ETH-UCY dataset, and 26% improvement on the PIE dataset, respectively, along with seven times fewer parameters than the existing state-of-the-art model (see Figure 1). Additionally, the model’s versatility allows it to generalize across different perspectives, such as Bird’s Eye View (BEV) and Ego-Vehicle View (EVV).

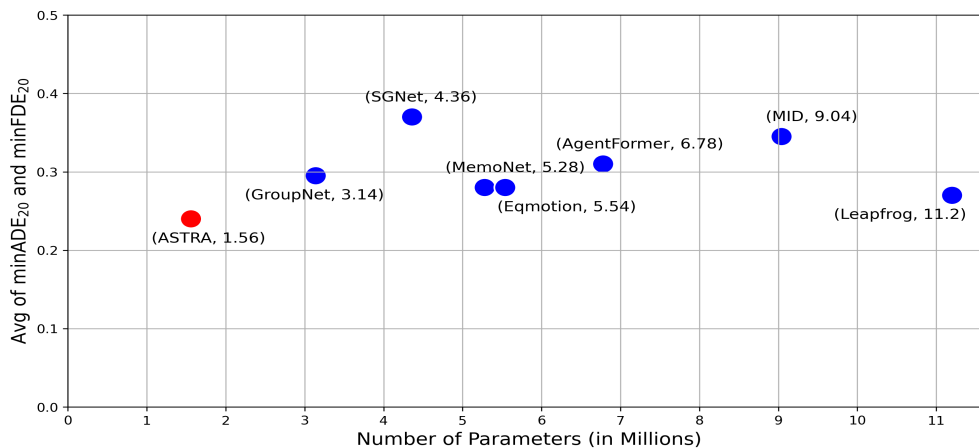


Figure 1: Comparison of average (minADE<sub>20</sub>/minFDE<sub>20</sub>) against the number of parameters for various models on the ETH-UCY dataset. Each point represents a different model, with the model name and number of parameters in millions indicated. Our model, ASTRA, achieves state-of-the-art results with the least number of parameters, demonstrating its efficiency and effectiveness in pedestrian trajectory forecasting.

## 1 Introduction

The pursuit of forecasting human trajectories is central, acting as a cornerstone for devising secure and interactive autonomous systems across various sectors. This endeavour is crucial in a wide array of applications, encompassing autonomous vehicles, drones, surveillance, human-robot interaction, and social robotics.

\*Visual Artificial Intelligence Laboratory, Oxford Brookes University, UK

†Indian Institute of Technology Bombay, India

Furthermore, it is crucial for predictive models to strike a balance between accuracy, dependability, and computational efficiency, given the imperative for these models to function on in-vehicle processing units with limited capabilities. The challenge of trajectory prediction involves estimating the future locations of agents within a scene, given its past trajectory. This estimation task can be tackled either through Bird’s Eye View (BEV) (Figure 2a) or Ego-Vehicle View (EVV) (Figure 2c) perspectives. This demands a comprehensive understanding of the scene, in addition to spatial, temporal, and social aspects that govern human movement and interaction.

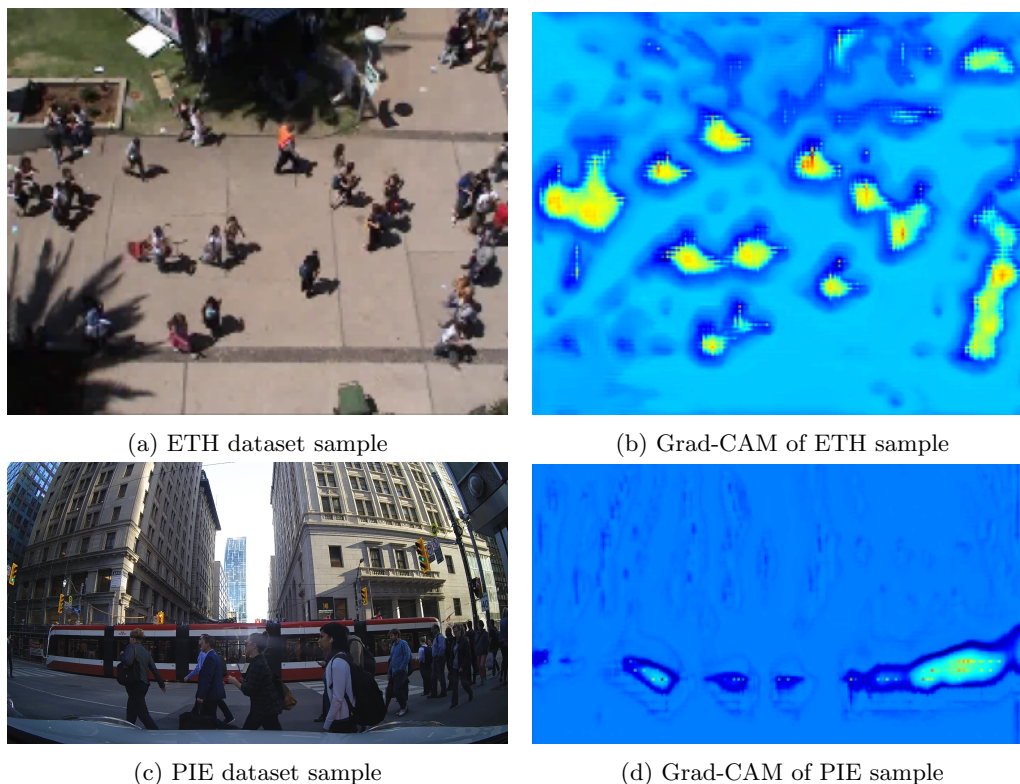


Figure 2: Sample images from the BEV dataset (ETH), and EVV dataset (PIE), along with their Grad-CAM representation from U-Net.

To solve the prediction problem, various building blocks, including RNNs, 3D-CNNs, and transformers, have been employed to address the temporal dimension, with transformers demonstrating superior efficacy [1, 2]. However, temporal modelling alone is unaware of the social behaviour of the agents within the scene, i.e. how agents interact with one another. In addressing the social dimension, methods such as Social Pooling [3] and Graph Neural Networks [4] (GNNs) have been explored, with GNN emerging as the most effective [5]. Some researchers have integrated both transformers and GNN, either sequentially or in parallel, to refine the prediction paradigm [6, 7, 8, 9]. However, these approaches entail heightened computational burdens due to the resource-intensive nature of both GNNs and transformers. Furthermore, transformers, by their inherent design, may pose potential challenges in preserving information, as they do not inherently accommodate the graph structure in their input. On the other hand, scene dimension, or scene embedding, delves into the interaction between an agent and its surroundings. [10] and [11] utilised semantic segmentation maps which enhanced the model’s grasp of environmental context. Another aspect across all surveyed papers, however, is their tendency to focus exclusively on either BEV or EVV, rarely considering both like [12]. This narrow focus becomes particularly problematic in, e.g., unstructured environments where a BEV might not be available, limiting the applicability of these methods.

In light of these challenges, this paper introduces a lightweight model, coined ASTRA (**A Scene-aware TRAnsfomer-based model for trajectory prediction**). By integrating a U-Net-based key-point extractor [13], ASTRA captures essential scene features without relying on explicit segmentation map annotations and alleviates the data requirements and preprocessing efforts highlighted earlier. This method also synergises the strengths of GNNs in representing the social dimension of the problem and of transformers in encoding its temporal dimension. Crucially, our approach processes spatial, temporal, and social dimensions concurrently, by embedding the graph structure into the token’s sequence prior to the attention mechanism, rendering the transformer graph-aware. The model does so while keeping the complexity of the model minimal. To refine the model’s ability to accurately learn trajectories, we implemented a modified version of the trajectory

prediction loss, incorporating a penalty component. This is in contrast to [14] which does not build a graph and does not preserve the social structure; they distinguish between self-agent and all other agents, then they treat all other agents the same without encoding the positional or structural encodings.

Furthermore, distinct from the vast majority of models in this domain, our model demonstrates generalisability by being applicable to both types of trajectory prediction datasets, BEV and EVV.

Our methodology underwent evaluation using renowned benchmark trajectory prediction datasets (Figure 2): ETH [15], UCY [16], and the PIE dataset [17]. The empirical findings highlight ASTRA’s outperforming the latest state-of-the-art methodologies. Notably, our method showcased significant improvements of 27% on the deterministic and 10% on the stochastic settings of the ETH and UCY datasets and 26% on PIE.

While maintaining high accuracy, ASTRA also features a significant reduction in the number of model’s parameters (Figure 1) - seven times fewer than the existing competing state-of-the-art model [18].

The paper’s highlights are as follows:

1. A lightweight model architecture that is seven times lighter than the existing state-of-the-art model, tailored for deployment on devices with limited processing capabilities while maintaining state-of-the-art predictive performance.
2. A loss-penalization strategy that enhances trajectory prediction, featuring a weighting trajectory loss function that dynamically adjusts penalty progression in response to prediction challenges.
3. Utilisation of the Scene-aware embeddings with a U-Net-based feature extractor to encode scene representations from frames, addressing a critical aspect often overlooked in recent works.
4. A graph-aware transformer encoder that contributes significantly to generating Agent-Scene aware embedding for improved prediction accuracy, ensuring informed inter-agent interaction capture.

## 2 Related Work

### 2.1 Trajectory Prediction

The trajectory prediction problem is usually approached in two ways: stochastic (multi-modal) predictions [18, 14, 19, 12] and deterministic (uni-modal) predictions [20, 21, 22]. The model produces only one prediction (most probable) per input motion in a deterministic setting. In contrast, a stochastic setting involves the model generating multiple predictions for each input motion. Stochastic approaches utilize generative techniques like Conditional Variational Auto-Encoders (CVAEs) [14, 12], Generative Adversarial Networks (GANs) [23], Normalizing Flows [24], or Denoising Diffusion Probabilistic Models [18] to introduce randomness into the prediction process, thereby generating diverse future trajectories with varying qualities for each pedestrian, aiming to elucidate the distribution of potential future coordinates of pedestrian trajectories. ASTRA also offers both deterministic and stochastic predictions like some of the previous works [5, 12, 25].

### 2.2 Social and Scene Dimension

The social dimension focuses on capturing agent-agent interactions, emphasizing how individuals or objects influence each other’s movements within a shared space. Notably, some methodologies incorporate social pooling, concurrently with attention mechanisms [3]. Algorithms in this domain predominantly leverage various forms of Graph Neural Networks (GNNs) to encapsulate the social dynamics among agents. Some methods employ a fully connected undirected graph, encompassing all scene agents [5, 26, 27]. This approach, albeit comprehensive, escalates exponentially with the number of agents (nodes). Conversely, other methods opt for sparsely connected graphs, establishing connections solely among agents within a proximal range, thereby reducing the linkage count substantially [28, 29, 25, 30]. In a similar vein, [14, 25] proposes sparse, directional graphs, predicated on the premise that different agent types possess varying perceptual ranges. Regarding the optimal depth of GNN layers, [31] advocate for deeper graphs to enhance performance. This stands in contrast to the findings of [30] and [32], who posit that two layers are optimal. Nevertheless, this depth increases computational demands, particularly when agent nodes are numerous, posing challenges for autonomous vehicle applications reliant on edge devices for processing.

The scene dimension, extracted from the video frames, includes the low-level representation of the physical environment, obstacles, and any elements that could affect the agent’s path, ensuring a comprehensive understanding of both social and environmental factors in predicting movement trajectories. [10] and [11] capture scene dimension with the help of semantic segmentation to delineate visual attributes of varied classes, subsequently elucidating their interrelations via attention. However, obtaining a panoptic segmentation mask, might not be always feasible. Also, this approach introduces a considerable dependency on

the availability of additional segmentation maps, presenting a challenge in terms of data requirements and preprocessing efforts.

## 2.3 Temporal Dimension

Understanding the trajectory history of an agent significantly augments the predictive accuracy regarding its potential future path. Predominantly, ego-camera-based models are tailored to shorter temporal horizons and employ 3D Convolutional Neural Networks (3D-CNNs) [28, 33]. Some research, instead, adopts Hidden Markov Models (HMMs) for temporal analysis [34]. For scenarios necessitating extended time horizon considerations, more intricate structures are proposed, including Transformers [14, 5, 35, 36] and various forms of Recurrent Neural Networks (RNNs) [29], including Long Short-Term Memory networks (LSTMs) [2, 37, 28] and Gated Recurrent Units (GRUs) [26]. Both Transformer and RNN-based models have exhibited superior performance, often achieving state-of-the-art results in this domain. However, some of these models tend to address the temporal dimension in isolation from the social context. This segregated approach potentially results in information loss and contributes to an increased computational load, necessitated by the addition of separate components to handle the social dimension. Consequently, there emerges a pressing demand for integrated models capable of concurrently processing both temporal and social dimensions. A promising direction in this regard is the development of graph-aware transformers, which encapsulate the essence of both temporal dynamics and social interactions within a unified framework.

## 2.4 Graph-aware Transformers

Graph-aware transformers aim to compound the benefits of graphs (with their associated social embeddings) and of transformers, with their acclaimed attention mechanism and temporal embeddings. Notably, these advancements have predominantly catered to graph-centric datasets like ACTOR [38] and CHAMELEON SQUIRREL [39]. Direct application of graph-aware transformers remains untouched in pedestrian trajectory forecasting, with prevalent methodologies leaning towards transformers processing embeddings emanating from graphs [6, 7, 8]. There has been a discernible preference for using GNN and transformer blocks, rather than fully-integrated graph-aware transformers.

A comprehensive evaluation of numerous contemporary graph-transformer models across three graph-centric datasets is conducted in [40]. The analysis reveals a consistent pattern: models employing Random Walk for structural encoding exhibit superior performance across all tested datasets. Building on this empirical evidence, our approach utilizes Random Walk to encode the pedestrian graph, which is then seamlessly integrated into the transformer architecture. This integration is designed to yield a graph-aware transformer, thereby enhancing the model’s capability to effectively capture and interpret complex pedestrian dynamics within various environments. To the best of the authors’ knowledge, this is the first work towards utilising a graph-aware transformer to solve the trajectory prediction problem, opposing many methods which use graphs along with transformers.

# 3 Methodology

**Problem Formulation.** The objective of pedestrian trajectory prediction is to forecast the future position of a pedestrian based on the observed historical sequence of the pedestrian’s positions. For this, the historical sequence of the pedestrians is provided as a sequence of coordinates  $\mathbf{X} = \{X_t^a \mid t \in (1, 2, \dots, T_{obs}); a \in (1, 2, \dots, A)\}$  related to  $A$  target agents extracted over the previous  $T_{obs}$  time instants. Here  $X_t^a$  is a pair of 2D coordinates  $\{x_t^a, y_t^a\}$  for BEV datasets (see Figure 2a), and a set of bounding box coordinates,  $\{x_{1,t}^a, y_{1,t}^a, x_{2,t}^a, y_{2,t}^a\}$ , for EVV datasets (see Figure 2c). In addition to the sequence coordinates  $\mathbf{X}$ ,  $T_{obs}$  input frames/images are also available, denoted as  $\mathbf{I} = \{I_t \mid t \in (1, 2, \dots, T_{obs})\}$ . The goal of ASTRA is to output deterministic or multi-modal trajectories of the pedestrian. In the deterministic setting, the problem consists of predicting the output prediction coordinates of the  $A$  agents in the subsequent  $T_{pred}$  future frames, formally  $\hat{\mathbf{Y}} = \{\hat{Y}_t^a \mid t \in (1, 2, \dots, T_{pred}); a \in (1, 2, \dots, A)\}$  where  $\hat{Y}_t^a$  denotes the coordinates of the agent  $a$  at a future time  $t$ , and the corresponding ground truth being  $\mathbf{Y} = \{Y_t^a \mid t \in (1, 2, \dots, T_{pred}); a \in (1, 2, \dots, A)\}$ . To output multimodal trajectories we need to learn a generative model, denoted by  $p_\theta(\mathcal{Y}|\mathbf{X}, \mathbf{I})$  which is parameterized by  $\theta$  and given  $\mathbf{X}$  and  $\mathbf{I}$ , outputs  $K$  predicted trajectories denoted by  $\mathcal{Y} = \{\hat{\mathbf{Y}}^{(1)}, \hat{\mathbf{Y}}^{(2)}, \dots, \hat{\mathbf{Y}}^{(K)}\}$ .

## 3.1 Components

The encoder part of our model consists of two main components: A scene-aware component and an agent-aware component. While the former is dedicated to encoding the scene, and encapsulating the contextual

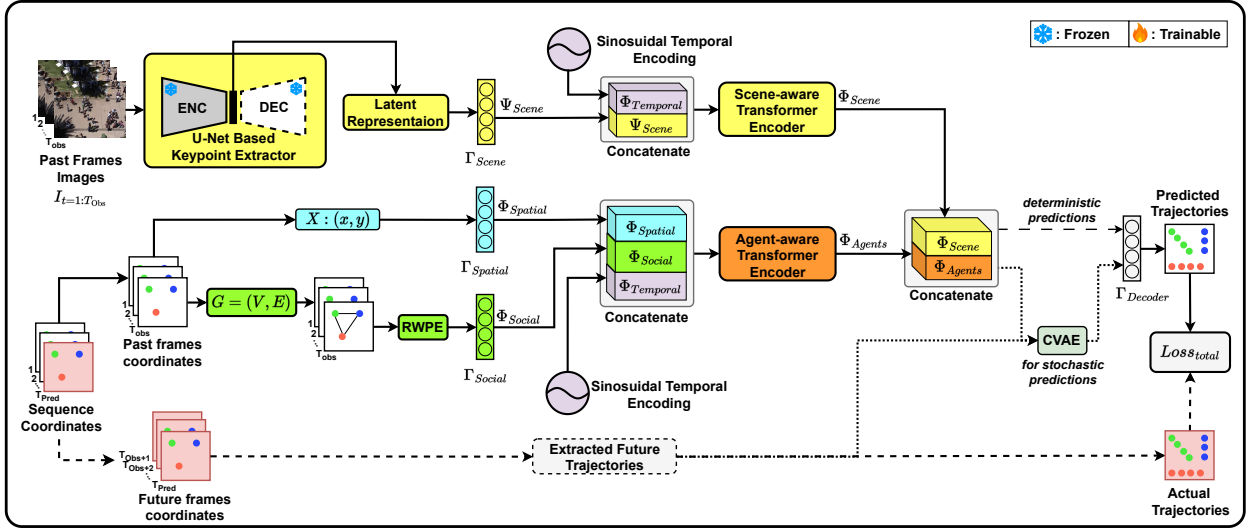


Figure 3: **Model Architecture.** Overview of ASTRA model architecture for pedestrian trajectory forecasting.

details, the latter focuses on encoding the spatial, temporal, and social dimensions of the agents, as shown in Figure 3. The output from these two components is aggregated before being decoded to generate single or multiple predicted future trajectories for deterministic/multi-modal predictions, respectively. In order to learn essential information about the scene’s spatial layout and the positional dynamics of agents within it, the U-Net [41] is pre-trained using the method detailed in [13] which utilizes a specialized loss function, Weighted Hausdorff Distance to learn a latent representation of the scene context (Figure 4). More sophisticated schemes to generate the scene representation, like transformer-based architectures, and fusing social representations via gated cross-attention can also be considered but we leave exploring possibly more effective and sophisticated architecture designs as future work. The Grad-CAM visualizations (Figures 2b and 2d) highlight this capability, showing that the pre-trained model pays attention to regions with a high likelihood of pedestrian activity. The U-Net-based keypoint extractor is frozen after the pretraining when used in ASTRA model architecture.

### 3.1.1 Temporal Encodings

To guide the network to model the temporal dimension, we add temporal encodings to the agents and scene to capture the temporal dependencies within the sequence of pedestrian trajectories from past frames, adopting a time encoder akin to the positional encoding found in the original Transformer architecture [42].

$$\Phi_{\text{Temporal}}(t, i) = \begin{cases} \sin\left(\frac{t}{10000^{2i/d}}\right) & \text{if } i \text{ is even} \\ \cos\left(\frac{t}{10000^{2i/d}}\right) & \text{if } i \text{ is odd} \end{cases} \quad (1)$$

where  $t$  is the time step,  $i$  is the dimension, and  $d$  is the dimensionality of the model.

### 3.1.2 Scene-aware embeddings.

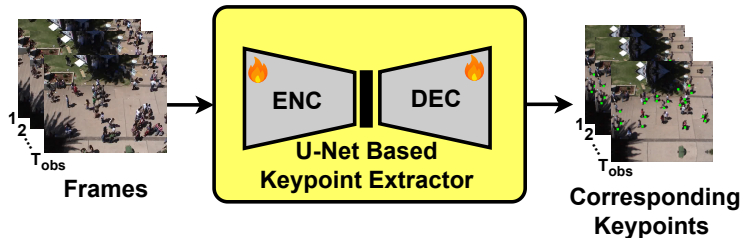


Figure 4: Pretraining U-Net based keypoint extractor.

A latent representation of pedestrian characteristics is obtained using a pre-trained U-Net encoder (Figure 3); this latent vector can include some crucial characteristics like spatial groupings and interactions with the environment. This step is crucial as the U-Net extractor possesses the proficiency to discern both labelled and unlabelled pedestrians, depicted in green and red, respectively in Figure 5a.

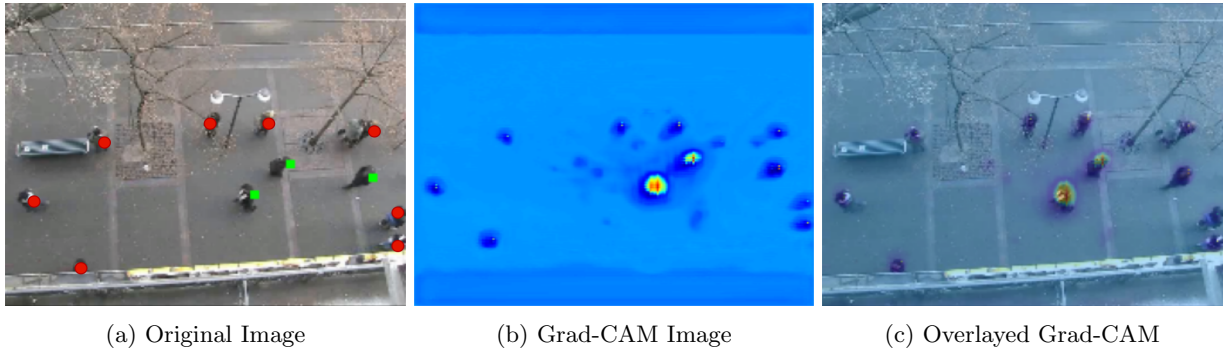


Figure 5: **Grad-CAM visualizations:** In (a), the red circle indicates unlabelled pedestrians, while the green square highlights labelled pedestrians. In (b), the U-Net-based keypoint extractor focuses on unlabelled pedestrians as well, thereby capturing scene context from them too.

### 3.1.3 Scene-aware transformer encoder.

The latent representation of all frames ( $\Psi_{\text{Scene}}$ ) is treated as input tokens to the scene-aware single-layer transformer encoder ( $T_{\text{Scene-aware}}$ ), which in turn generates scene-aware embeddings ( $\Phi_{\text{Scene}}$ ) for each frame. The single-layer transformer encoder architectural choice significantly contributes to the lightweight nature of our model. The resulting scene embedding is:

$$\Psi_{\text{Scene}} = \Gamma_{\text{Scene}}(\Upsilon_{\text{Encoder}}(\mathbf{I})) \quad (2)$$

$$\Phi_{\text{Scene}} = T_{\text{Scene-aware}}([\Psi_{\text{Scene}}; \Phi_{\text{Temporal}}]) \quad (3)$$

where past input frame images projected using a Multi-Layer Perceptron (MLP) layer ( $\Gamma_{\text{Scene}}$ ), and  $\Upsilon_{\text{Encoder}}(\cdot)$  denotes the encoder part of the U-Net.

The temporal encoding  $\Phi_{\text{Temporal}}$ , crucial for capturing the temporal dynamics within the observed frames, adopts the design of the traditional positional encoding [42] and follows the work of [14].

### 3.1.4 Agent-aware embeddings.

The second component is dedicated to encoding the different dimensions of each agent for all agents in the scene.

The spatial coordinates  $\mathbf{X}$  of each agent are linearly projected to a latent space using an MLP layer ( $\Gamma_{\text{Spatial}}$ ) to get spatial encoding ( $\Phi_{\text{Spatial}}$ )

$$\Phi_{\text{Spatial}} = \Gamma_{\text{Spatial}}(\mathbf{X}) \quad (4)$$

Spatial embeddings are not enough to capture the full information about the agents. If two agents in two frames have the same location in the image, their spatial embedding will be the same. Hence, temporal encoding (equation in Supplementary material) is also included to distinguish them.

Having the spatial and temporal dimensions of the agents is still not enough to understand their interaction in the scene. To capture the social dimension in this multi-agent environment, we generate a fully connected undirected graph between agents, in which the nodes are the agents' locations, and the edges between agents are the reciprocal of the distance. Consequently, the closer the agents are to each other, the stronger the link between them. Formally, we represent the social dimension using a graph  $G = (V, E)$ , where  $V$  is the set of agents and  $E$  is the collection of edges, with weights

$$e_{ij} = \frac{1}{d(v_i, v_j)} \quad (5)$$

where  $d(v_i, v_j)$  is the distance between agents  $v_i$  and  $v_j$ .

Subsequently, Random Walk Positional Encodings (RWPEs) [43] is used to capture the structural relationships between nodes in the graph, such as their proximity to each other and the number of paths between them. These RWPEs are further projected to latent space using a separate MLP ( $\Gamma_{\text{Social}}$ ) to get social encodings ( $\Phi_{\text{Social}}$ ), mathematically:

$$\Phi_{\text{Social}} = \Gamma_{\text{Social}}(\text{RWPE}(\mathbf{G})) \quad (6)$$

This preserves the graph structure of the agents while making the transformer encoder graph-aware. Furthermore, our method empowers the network to determine the significance of each agent relative to others autonomously.

While we do not claim to be the first to use transformers or graphs, we claim that we are the first to integrate RWPE directly into transformer tokens, creating a graph-aware transformer in the context of trajectory prediction, which has proven successful, outperforming the state-of-the-art (SOTA).

### 3.1.5 Agent-aware transformer encoder.

After calculating the spatial, temporal and social representations for each agent, our model concatenates them. This concatenated vector is then fed into an agent-aware single-layer transformer encoder ( $T_{\text{Agent-aware}}$ ) that generates agent-aware embedding ( $\Phi_{\text{Agents}}$ ).

$$\Phi_{\text{Agents}} = T_{\text{Agent-aware}}([\Phi_{\text{Spatial}}; \Phi_{\text{Temporal}}; \Phi_{\text{Social}}]) \quad (7)$$

### 3.1.6 Decoder.

To generate multiple stochastic trajectories, we learn a generative model,  $p_{\theta}(\mathcal{Y}|\mathbf{X}, \mathbf{I})$  for which we adopted CVAE(Conditional Variational Auto Encoder). We train CVAE to learn the inherent distribution of future target trajectories conditioned on observed past trajectories, by utilizing a latent variable  $Z$ . CVAE consists of three components - prior network ( $p_{\theta}(Z|X, I)$ ), recognition network ( $q_{\phi}(Z|Y, X, I)$ ) and generation network ( $g_{\nu}(\tilde{Y}|Z)$ ), parameterized by  $\theta$ ,  $\phi$  and  $\nu$  respectively. Here  $\tilde{Y}$  is the output of the generation network and is the latent representation of the future trajectories. To generate future trajectories, we pass  $\tilde{Y}$  to the MLP decoder ( $\Gamma_{\text{Decoder}}$ ).

For deterministic predictions, CVAE is skipped and the outputs of both the scene transformer ( $\Phi_{\text{Scene}}$ ) and the agents' transformer ( $\Phi_{\text{Agents}}$ ) are concatenated and directly passed through an MLP decoder ( $\Gamma_{\text{Decoder}}$ ) to produce future trajectories ( $\hat{Y}$ ) of the agents in the future frames as shown in Figure 3, namely:

$$\hat{Y} = \Gamma_{\text{Decoder}}([\Phi_{\text{Scene}}; \Phi_{\text{Agents}}]) \quad (8)$$

### 3.1.7 Weighted trajectory loss function.

We introduce a weighted-penalty strategy that can be applied to common loss functions used in trajectory prediction such as MSE and Smooth L1 Loss. The application of this strategy is through a dynamic penalty function  $w(t)$ , designed to escalate or de-escalate the significance of prediction errors as one moves further into the future. The definition of the weighted loss function is given by:

$$L_{\text{weighted}}(\hat{Y}, Y) = \sum_{t=1}^{T_{\text{pred}}} w(t) \cdot L(\hat{Y}_t, Y_t), \quad (9)$$

where  $\hat{Y}$  and  $Y$  are the predicted and actual trajectories respectively,  $T_{\text{pred}}$  denotes the number of prediction timesteps,  $w(t)$  represents the dynamic weighting function at time  $t$ , and  $L(\hat{Y}_t, Y_t)$  is the predefined loss function (e.g., MSE or SmoothL1 Loss) applied to the predicted and true positions at each time step  $t$ .

In time series data, as we move further into the future relative to the last observed data, the drift in predictions tends to increase, leading to higher errors. Motivated by this intuition, we initially penalized the predictions using linear and quadratic loss functions. These approaches showed improvements in overall prediction accuracy. However, upon closer analysis of the results, we observed that in some trajectories, there was a noticeable offset in the earlier parts of the predictions. To address this issue, we experimented with a parabolic weighting function for the penalty. Empirically, this approach outperformed the linear and quadratic strategies, yielding the most balanced and accurate predictions across the trajectories.

The weight function  $w(t)$  is designed to be versatile, accommodating a spectrum of mathematical formulations that align with the specific needs of the predictive model. It is generically defined as:

$$w(t) = f(t, T_{\text{pred}}, \alpha, \beta), \quad (10)$$

where  $\alpha$  and  $\beta$  are parameters that establish the bounds of the weighting function, and  $f$  is an adaptable function that governs the progression of weights at each timestep  $t$ .

In particular, the function  $w(t)$  may be selected from various mathematical forms, such as linear, parabolic, or quadratic, which are discussed in greater detail within the supplementary materials. The choice of function enables the model to adjust the penalty progression in alignment with the anticipated prediction challenge at each timestep.

To generate multi-modal trajectories, the entire ASTRA model is optimized using Equation 12. The prior distribution ( $p_\theta(z|X, I)$ ) is parameterized by  $\mathcal{N}(\mu_z^p, (\sigma_z^p)^2)$ . The approximate posterior distribution ( $q_\phi(z|Y, X, I)$ ) is parameterized by  $\mathcal{N}(\mu_z^q, (\sigma_z^q)^2)$ , where  $\mu_z^p$  and  $(\sigma_z^p)^2$  represent the mean and variance of the prior distribution and  $\mu_z^q$  and  $(\sigma_z^q)^2$  represent the mean and variance of the posterior distribution. During Training, we sample latent variable( $z$ ) from the recognition network (posterior distribution) and fed it to the generation network, whereas during testing we sample  $z$  from the prior network (prior distribution). We use the reparameterization trick to sample  $z$  through the mean and variance pairs of  $(\mu_z^p, (\sigma_z^p)^2)$  and  $(\mu_z^q, (\sigma_z^q)^2)$ , respectively. KL divergence term help in minimizing the difference between the distribution of latent variable( $z$ ) of prior and recognition network. During inference,  $K$  samples are drawn from the learned distribution and decoded to future trajectories.

$$\mathcal{L}_{\text{final}} = L_{\text{weighted}}(\hat{\mathbf{Y}}, \mathbf{Y}) + D_{KL}(q_\phi(Z|Y, X, I)||p_\theta(Z|X, I)) \quad (11)$$

$$\mathcal{L}_{\text{final}} = L_{\text{weighted}}(\hat{\mathbf{Y}}, \mathbf{Y}) + D_{KL}(\mathcal{N}(\mu_{z_q}, \sigma_{z_q})||\mathcal{N}(\mu_{z_p}, \sigma_{z_p})) \quad (12)$$

## 4 Experiments

### 4.1 Datasets and Evaluation Protocol

For a comprehensive evaluation, we benchmarked our model on three trajectory prediction datasets; namely, ETH [15], UCY [16], and PIE dataset [17]. **ETH** and **UCY** offer a bird’s-eye view of pedestrian dynamics in urban settings, including five datasets with 1,536 pedestrians across four scenes. For evaluation, we used their standard protocol; leave-one-out strategy, observing eight time steps (3.2s) and predicting the following 12 steps (4.8s).

In contrast, the **PIE dataset** provides an Ego-vehicle perspective, containing over 6 hours of ego-centric driving footage, along with bounding box annotations for traffic objects, action labels for pedestrians, and ego-vehicle sensor information [17]. A total of 1,842 pedestrian samples are considered with the following split: Training(50%), Validation(40%) and Testing(10%)[17]. Model performance is evaluated based on a shorter observational window of 0.5 seconds and a prediction window of 1 second, providing insights into the model’s capability in rapidly evolving traffic scenarios[2].

### 4.2 Evaluation Metrics

We used the standard evaluation metrics of ADE and FDE for ETH-UCY deterministic settings and minADE and minFDE for their stochastic settings. ADE, FDE, CADE, CFDE, ARB and FRB for PIE dataset, the supplementary material explains these metrics.

### 4.3 Setting up the experiments

We trained the model on the ETH-UCY and PIE datasets using the AdamW optimizer with a weight decay of  $5 \times 10^{-4}$  for 200 epochs. The initial learning rate was set to  $1 \times 10^{-3}$ , and a cosine annealing scheduler was employed. Training was conducted on a NVIDIA DGX A100 machine, equipped with 8 GPUs, each having 80 GB of memory.

### 4.4 FLOPS

For AgentFormer, the model has approximately 3.084 GFLOPs, whereas ASTRA is comparatively lighter with 1.7 MFLOPs (including U-Net and CVAE), highlighting ASTRA’s computational efficiency. With pretrained U-net the model has 839 KFLOPs and without including the CVAE, model has 16 KFLOPs.

### 4.5 Discussing the Results

#### 4.5.1 Quantitative Results.

For ETH-UCY, we compared our model results against several baselines. These comparisons are presented in Table 1 and Table 2, which contains results primarily sourced from the EqMotion (CVPR 2023) [5] for deterministic predictions and LeapFrog (CVPR 2023) [18] for stochastic predictions respectively. It is important to note that to provide a thorough comparative framework, we independently computed and included additional models [46, 12] to their respective tables as they were not originally part of the EqMotion or LeapFrog analysis. Our model significantly advances the state-of-the-art on ETH-UCY, outperforming



Table 1: **Deterministic Results:** ADE/FDE results for ETH-UCY baselines. Best in **bold**, second best underlined.

Model	ETH	Hotel	Univ	Zara1	Zara2	Average
Linear	1.33/2.94	0.39/0.72	0.82/1.59	0.62/1.21	0.77/1.48	0.79/1.59
S-LSTM[22]	1.09/2.35	0.79/1.76	0.67/1.40	0.47/1.00	0.56/1.17	0.72/1.54
S-Attention[44]	1.39/2.39	2.51/2.91	1.25/2.54	1.01/2.17	0.88/1.75	1.41/2.35
SGAN-ind[45]	1.13/2.21	1.01/2.18	0.60/1.28	0.42/0.91	0.52/1.11	0.74/1.54
Traj++[25]	1.02/2.00	0.33/0.62	<u>0.53</u> /1.19	0.44/0.99	0.32/0.73	0.53/1.11
TransF[35]	1.03/2.10	0.36/0.71	<u>0.53</u> /1.32	0.44/1.00	0.34/0.76	0.54/1.17
MemoNet[19]	1.00/2.08	0.35/0.67	0.55/1.19	0.46/1.00	0.37/0.82	0.55/1.15
SGNet[46]	<u>0.81</u> / <u>1.60</u>	0.41/0.87	0.58/1.24	<u>0.37</u> / <u>0.79</u>	0.31/0.68	0.56/1.04
EqMotion[5]	0.96/1.92	<u>0.30</u> / <u>0.58</u>	<b>0.50</b> / <b>1.10</b>	0.39/0.86	<u>0.30</u> / <u>0.68</u>	<u>0.49</u> / <u>1.03</u>
ASTRA (Ours)	<b>0.47</b> / <b>0.82</b>	<b>0.29</b> / <b>0.56</b>	0.55/ <b>1.00</b>	<b>0.34</b> / <b>0.71</b>	<b>0.24</b> / <b>0.41</b>	<b>0.38</b> / <b>0.70</b>

Table 2: **Stochastic Results:** minADE<sub>20</sub> and minFDE<sub>20</sub> results for ETH-UCY baselines. Best in **bold**, second best underlined. NP- means unpenalised.

Model	ETH	Hotel	Univ	Zara1	Zara2	Average
Social-GAN [45]	0.87/1.62	0.67/1.37	0.76/1.52	0.35/0.68	0.42/0.84	0.61/1.21
NMMP [47]	0.61/1.08	0.33/0.63	0.52/1.11	0.32/0.66	0.43/0.85	0.41/0.82
STAR [48]	0.36/0.65	0.17/0.36	0.31/0.62	0.29/0.52	0.22/0.46	0.26/0.53
PECNet [49]	0.54/0.87	0.18/0.24	0.35/0.60	0.22/0.39	0.17/0.30	0.29/0.48
Trajectron++ [25]	0.61/1.02	0.19/0.28	0.30/0.54	0.24/0.42	0.18/0.32	0.30/0.51
BiTrap-NP [12]	0.55/0.95	0.17/0.28	0.25/0.47	0.22/0.44	0.16/0.33	0.27/0.49
MemoNet [19]	0.40/0.61	<b>0.11</b> / <b>0.17</b>	0.24/ <u>0.43</u>	0.18/0.32	0.14/0.24	<u>0.21</u> /0.35
GroupNet [50]	0.40/0.76	<u>0.12</u> / <u>0.18</u>	<b>0.22</b> / <b>0.41</b>	<u>0.17</u> /0.31	<b>0.12</b> /0.24	<u>0.21</u> /0.38
SGNet [46]	0.47/0.77	0.20/0.38	0.33/0.62	0.18/0.32	0.15/0.28	0.27/0.47
MID [51]	0.46/0.73	0.15/0.25	0.26/0.49	0.21/0.39	0.17/0.33	0.25/0.44
Agentformer [14]	0.45/0.75	0.14/0.22	0.25/0.45	0.18/0.30	0.14/0.24	0.23/0.39
EqMotion [5]	0.40/0.61	<u>0.12</u> / <u>0.18</u>	<u>0.23</u> / <u>0.43</u>	0.18/0.32	<u>0.13</u> /0.23	<u>0.21</u> /0.35
Leapfrog [18]	0.39/0.58	<b>0.11</b> / <b>0.17</b>	0.26/ <u>0.43</u>	0.18/ <u>0.26</u>	<u>0.13</u> /0.22	<u>0.21</u> /0.33
ASTRA(Non Penalised)	0.37/0.49	0.24/0.34	0.37/0.52	0.23/0.32	0.16/0.23	0.27/0.38
ASTRA(Without Frame Encoding)	<u>0.29</u> / <u>0.39</u>	0.18/0.29	0.29/ <u>0.43</u>	<u>0.17</u> / <u>0.26</u>	0.14/ <u>0.2</u>	<u>0.21</u> / <u>0.31</u>
ASTRA(With Frame Encoding)	<b>0.27</b> / <b>0.36</b>	0.17/0.25	0.28/ <b>0.41</b>	<b>0.15</b> / <b>0.23</b>	<u>0.13</u> / <b>0.16</b>	<b>0.20</b> / <b>0.28</b>

the EqMotion [5] by improving predictive accuracy by approximately 27% on average for deterministic predictions as shown in Table 1 and approximately 10% on average improvement over LeapFrog[18] for stochastic predictions as shown in Table 2, highlighting the efficacy of our approach in diverse scenarios. We also highlight the effectiveness of utilizing frame encodings from U-Net, as demonstrated in Table 2.

Similarly, we benchmarked our model against various established models for the PIE dataset. The comparative analysis is summarized in Table 4, with the reference results taken from the PedFormer [2], demonstrating an average improvement of 26%.

#### Trainable Parameters and Computational Efficiency .

Regarding the computational side, ASTRA has seven times fewer trainable parameters than the existing SOTA model LeapFrog [18] as shown in Figure 1. It is important to note that the parameter count reported for ASTRA in Figure 1 includes the parameters from the U-Net, which is otherwise actually frozen during the trajectory prediction phase. The full ASTRA architecture with all the components included involves 1.56M parameters and 1.77M FLOPs, which is substantially more efficient than AgentFormer’s 6.78M parameters and 3.08G FLOPs. Even configurations of ASTRA without U-Net pretraining for deterministic predictions can be as compact as 13.52K parameters with minimal FLOPs (15.87K), indicating that we can flexibly adapt ASTRA’s complexity to meet strict resource constraints. A more detailed comparison for the same is given in [supplementary](#).

#### 4.5.2 Qualitative results.

We can clearly see the results of our prediction from Figure 6 for deterministic predictions and Figure 8 for stochastic prediction. Figure 7 exemplifies the proximity of our model’s results to the ground truth, it also shows how using the weighted penalty strategy has yielded better results than the unpenalised one, highlighting the improved effectiveness of our strategy.

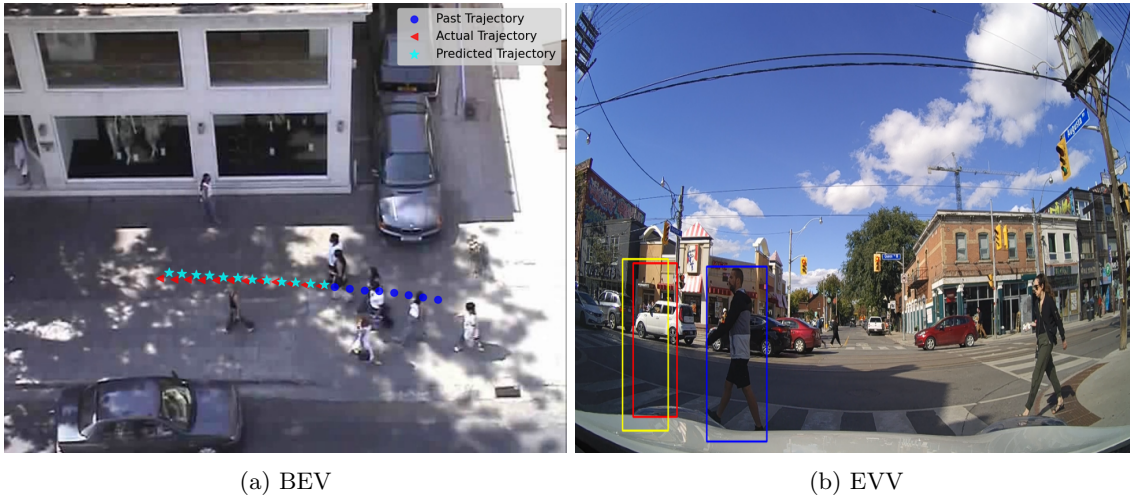


Figure 6: Sample images of the deterministic prediction from BEV datasets (a.) (ETH and UCY) and EVV dataset (b.) (PIE). The Red and Yellow bounding box indicates the ground-truth and predicted final position respectively and the Blue bounding box indicates the start position.

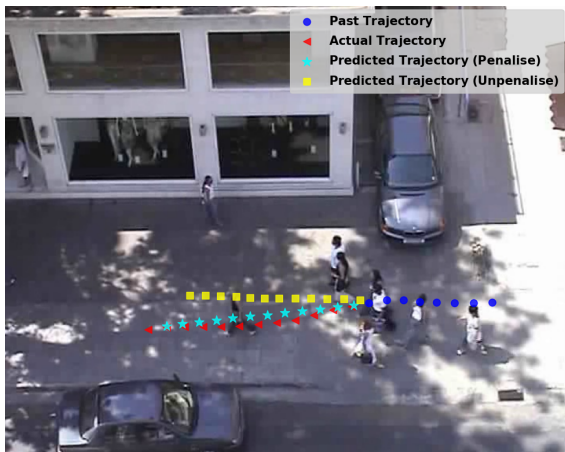


Figure 7: Visual comparison of penalised and unpenalised loss on ETH-UCY, showing the enhanced performance of the former.



Figure 8: Sample images of the stochastic predictions from ETH-UCY Dataset.

Table 3: **Ablation:** ADE/FDE &  $\min\text{ADE}_{20}/\min\text{FDE}_{20}$  with variations in ASTRA’s model components on UNIV dataset (where  $\checkmark$ : Component enabled,  $\times$ : Component disabled)

Spatial	Temporal	Augmentation	Social	U-Net Features	ADE/FDE	$\min\text{ADE}_{20}/\min\text{FDE}_{20}$
$\checkmark$	$\times$	$\times$	$\times$	$\times$	1.05/1.66	0.43/0.63
$\checkmark$	$\checkmark$	$\times$	$\times$	$\times$	0.86/1.47	0.39/0.54
$\checkmark$	$\checkmark$	$\checkmark$	$\times$	$\times$	0.67/1.17	0.31/0.48
$\checkmark$	$\checkmark$	$\checkmark$	$\checkmark$	$\times$	0.66/1.12	0.29/0.43
$\checkmark$	$\checkmark$	$\checkmark$	$\checkmark$	$\checkmark$	0.55/1.00	0.28/0.41

### 4.5.3 Ablation studies.

In the ablation study presented in Table 3, we evaluated the contribution of each component in our trajectory prediction model to ascertain their individual and collective impact on the performance metrics on the ETH-UCY (UNIV) dataset. Initially, the model incorporated only spatial information, which served as a baseline for subsequent enhancements. The sequential integration of temporal and social components yielded successive improvements, demonstrating their respective significance in capturing the dynamics of agent movement. The addition of the data augmentation technique (detailed in the supplementary material) further refined the model’s performance, illustrating the value of varied training samples in enhancing generalization capabilities. Moreover, the incorporation of U-Net features contributed to a substantial leap

forward, highlighting the importance of context-aware embeddings in accurately forecasting agent trajectories. This progression emphasizes the synergistic effect of combining heterogeneous data representations to capture the nuanced patterns of movement within a scene.

The ablation study also extended to the evaluation of loss functions, comparing the effects of penalised versus unpenalised approaches. Penalized loss functions, designed to focus the model’s attention on more critical prediction horizons, proved to be more effective in refining the predictive accuracy, as outlined in Table 5 and in Table 2 (ASTRA(NP)) for deterministic and stochastic setting respectively and the same can be observed in Figure 7.

Table 4: Results for PIE dataset.

Model	CADE	CFDE	ARB	FRB
FOL[52]	73.87	164.53	78.16	143.69
FPL[53]	56.66	132.23	-	-
B-LSTM[54]	27.09	66.74	37.41	75.87
PIE <sub>traj</sub> [17]	21.82	53.63	27.16	55.39
PIE <sub>full</sub> [17]	19.50	45.27	24.40	49.09
BiPed[55]	15.21	35.03	19.62	39.12
PedFormer[2]	<u>13.08</u>	<u>30.35</u>	<b>15.27</b>	<u>32.79</u>
ASTRA(Ours)	<b>9.91</b>	<b>22.42</b>	<u>18.32</u>	<b>17.07</b>

Table 5: **Ablation:** ADE/FDE for penalised vs. unpenalised loss functions on UNIV dataset using SOTA ASTRA’s configuration

Loss	Normal	Penalised
MSE	0.58/1.13	0.57/1.00
SmoothL1	0.57/1.15	0.55/1.00

## 5 Conclusion

We presented ASTRA, a model in the domain of pedestrian trajectory prediction, that outperforms the existing state-of-the-art models. This advancement renders ASTRA particularly suitable for deployment on devices with limited processing capabilities, thereby broadening the applicability of high-accuracy trajectory prediction technologies. ASTRA’s adeptness in handling both BEV and EVV modalities further solidifies its applicability in diverse operational contexts. With the ability to produce deterministic and stochastic results, it enhances the predictive robustness and situational awareness of autonomous systems. Moving forward, we aim to extend the capabilities of the ASTRA model beyond pedestrian trajectory prediction to encompass a broader range of non-human agents. This expansion will involve adapting the model to understand and predict the movements of various entities within shared environments using more sophisticated architectural design choices to encode the scene and its fusion with social dimension. By broadening our focus, we hope to contribute to the development of truly comprehensive and adaptive systems capable of navigating the complexities of real-world interactions among a wide array of agents.

## References

- [1] F. Giuliari, I. Hasan, M. Cristani, and F. Galasso, “Transformer networks for trajectory forecasting,” in *2020 25th international conference on pattern recognition (ICPR)*. IEEE, 2021, pp. 10 335–10 342.
- [2] A. Rasouli and I. Kotseruba, “Pedformer: Pedestrian behavior prediction via cross-modal attention modulation and gated multitask learning,” in *2023 IEEE International Conference on Robotics and Automation (ICRA)*. IEEE, 2023, pp. 9844–9851.
- [3] B. Pang, T. Zhao, X. Xie, and Y. N. Wu, “Trajectory prediction with latent belief energy-based model,” in *2021 IEEE/CVF Conference on Computer Vision and Pattern Recognition (CVPR)*, 2021, pp. 11 809–11 819.
- [4] T. N. Kipf and M. Welling, “Semi-supervised classification with graph convolutional networks,” *CoRR*, vol. abs/1609.02907, 2016. [Online]. Available: <http://arxiv.org/abs/1609.02907>
- [5] C. Xu, R. T. Tan, Y. Tan, S. Chen, Y. G. Wang, X. Wang, and Y. Wang, “Eqmotion: Equivariant multi-agent motion prediction with invariant interaction reasoning,” in *Proceedings of the IEEE/CVF Conference on Computer Vision and Pattern Recognition*, 2023, pp. 1410–1420.
- [6] L. Li, M. Pagnucco, and Y. Song, “Graph-based spatial transformer with memory replay for multi-future pedestrian trajectory prediction,” in *Proceedings of the IEEE/CVF Conference on Computer Vision and Pattern Recognition*, 2022, pp. 2231–2241.
- [7] X. Chen, H. Zhang, Y. Hu, J. Liang, and H. Wang, “Vnagt: Variational non-autoregressive graph transformer network for multi-agent trajectory prediction,” *IEEE Transactions on Vehicular Technology*, pp. 1–12, 2023.
- [8] X. Jia, P. Wu, L. Chen, Y. Liu, H. Li, and J. Yan, “Hdgt: Heterogeneous driving graph transformer for multi-agent trajectory prediction via scene encoding,” *IEEE transactions on pattern analysis and machine intelligence*, 2023.
- [9] Y. Liu, L. Yao, B. Li, X. Wang, and C. Sammut, “Social graph transformer networks for pedestrian trajectory prediction in complex social scenarios,” in *Proceedings of the 31st ACM International Conference on Information & Knowledge Management*, ser. CIKM ’22. New York, NY, USA: Association for Computing Machinery, 2022, p. 1339–1349. [Online]. Available: <https://doi.org/10.1145/3511808.3557455>
- [10] A. Rasouli, M. Rohani, and J. Luo, “Bifold and semantic reasoning for pedestrian behavior prediction,” in *Proceedings of the IEEE/CVF International Conference on Computer Vision*, 2021, pp. 15 600–15 610.
- [11] K. Mangalam, Y. An, H. Girase, and J. Malik, “From goals, waypoints & paths to long term human trajectory forecasting,” in *Proceedings of the IEEE/CVF International Conference on Computer Vision*, 2021, pp. 15 233–15 242.
- [12] Y. Yao, E. Atkins, M. Johnson-Roberson, R. Vasudevan, and X. Du, “Bitrap: Bi-directional pedestrian trajectory prediction with multi-modal goal estimation,” *IEEE Robotics and Automation Letters*, vol. 6, no. 2, pp. 1463–1470, 2021.
- [13] J. Ribera, D. Guera, Y. Chen, and E. J. Delp, “Locating objects without bounding boxes,” in *Proceedings of the IEEE/CVF Conference on Computer Vision and Pattern Recognition*, 2019, pp. 6479–6489.
- [14] Y. Yuan, X. Weng, Y. Ou, and K. Kitani, “Agentformer: Agent-aware transformers for socio-temporal multi-agent forecasting,” in *Proceedings of the IEEE/CVF International Conference on Computer Vision (ICCV)*, 2021.
- [15] S. Pellegrini, A. Ess, K. Schindler, and L. van Gool, “You’ll never walk alone: Modeling social behavior for multi-target tracking,” in *2009 IEEE 12th International Conference on Computer Vision*, 2009, pp. 261–268.
- [16] A. Lerner, Y. Chrysanthou, and D. Lischinski, “Crowds by example,” *Computer Graphics Forum*, vol. 26, no. 3, pp. 655–664, 2007. [Online]. Available: <https://onlinelibrary.wiley.com/doi/abs/10.1111/j.1467-8659.2007.01089.x>
- [17] A. Rasouli, I. Kotseruba, T. Kunic, and J. Tsotsos, “Pie: A large-scale dataset and models for pedestrian intention estimation and trajectory prediction,” in *2019 IEEE/CVF International Conference on Computer Vision (ICCV)*, 2019, pp. 6261–6270.

- [18] W. Mao, C. Xu, Q. Zhu, S. Chen, and Y. Wang, “Leapfrog diffusion model for stochastic trajectory prediction,” in *Proceedings of the IEEE/CVF Conference on Computer Vision and Pattern Recognition (CVPR)*, June 2023, pp. 5517–5526.
- [19] C. Xu, W. Mao, W. Zhang, and S. Chen, “Remember intentions: Retrospective-memory-based trajectory prediction,” pp. 6488–6497, June 2022.
- [20] D. Helbing and P. Molnar, “Social force model for pedestrian dynamics,” *Physical review E*, vol. 51, no. 5, p. 4282, 1995.
- [21] S. Pellegrini, A. Ess, K. Schindler, and L. Van Gool, “You’ll never walk alone: Modeling social behavior for multi-target tracking,” in *2009 IEEE 12th international conference on computer vision*. IEEE, 2009, pp. 261–268.
- [22] A. Alahi, K. Goel, V. Ramanathan, A. Robicquet, L. Fei-Fei, and S. Savarese, “Social lstm: Human trajectory prediction in crowded spaces,” in *Proceedings of the IEEE Conference on Computer Vision and Pattern Recognition (CVPR)*, June 2016.
- [23] L. Huang, J. Zhuang, X. Cheng, R. Xu, and H. Ma, “Sti-gan: Multimodal pedestrian trajectory prediction using spatiotemporal interactions and a generative adversarial network,” *IEEE Access*, vol. 9, pp. 50 846–50 856, 2021.
- [24] A. Bhattacharyya, C. Straehle, M. Fritz, and B. Schiele, “Haar wavelet based block autoregressive flows for trajectories,” *CoRR*, vol. abs/2009.09878, 2020. [Online]. Available: <https://arxiv.org/abs/2009.09878>
- [25] T. Salzmann, B. Ivanovic, P. Chakravarty, and M. Pavone, “Trajectron++: Dynamically-feasible trajectory forecasting with heterogeneous data,” in *Computer Vision–ECCV 2020: 16th European Conference, Glasgow, UK, August 23–28, 2020, Proceedings, Part XVIII 16*. Springer, 2020, pp. 683–700.
- [26] T. Gilles, S. Sabatini, D. Tsishkou, B. Stanciulescu, and F. Moutarde, “Gohome: Graph-oriented heatmap output for future motion estimation,” *arXiv preprint arXiv:2109.01827*, 2021.
- [27] V. Kosaraju, A. Sadeghian, R. Martín-Martín, I. D. Reid, S. H. Rezatofighi, and S. Savarese, “Social-bigat: Multimodal trajectory forecasting using bicycle-gan and graph attention networks,” in *NeurIPS*, 2019.
- [28] J. Fang, D. Yan, J. Qiao, J. Xue, and H. Yu, “Dada: Driver attention prediction in driving accident scenarios,” *IEEE Transactions on Intelligent Transportation Systems*, 2021.
- [29] H. Girase, H. Gang, S. Malla, J. Li, A. Kanehara, K. Mangalam, and C. Choi, “Loki: Long term and key intentions for trajectory prediction,” in *Proceedings of the IEEE/CVF International Conference on Computer Vision*, 2021, pp. 9803–9812.
- [30] X. Weng, Y. Yuan, and K. Kitani, “Ptp: Parallelized tracking and prediction with graph neural networks and diversity sampling,” *IEEE Robotics and Automation Letters*, vol. 6, pp. 4640–4647, 7 2021.
- [31] R. Addanki, P. W. Battaglia, D. Budden, A. Deac, J. Godwin, T. Keck, W. L. S. Li, A. Sanchez-Gonzalez, J. Stott, S. Thakoor *et al.*, “Large-scale graph representation learning with very deep gnn and self-supervision,” *arXiv preprint arXiv:2107.09422*, 2021.
- [32] B. Liu, E. Adeli, Z. Cao, K.-H. Lee, A. Shenoi, A. Gaidon, and J. C. Niebles, “Spatiotemporal relationship reasoning for pedestrian intent prediction,” *IEEE Robotics and Automation Letters*, vol. 5, no. 2, pp. 3485–3492, 2020.
- [33] I. Kotseruba, A. Rasouli, and J. K. Tsotsos, “Benchmark for evaluating pedestrian action prediction,” in *2021 IEEE Winter Conference on Applications of Computer Vision (WACV)*, 2021, pp. 1257–1267.
- [34] W. Cai, G. He, J. Hu, H. Zhao, Y. Wang, and B. Gao, “A comprehensive intention prediction method considering vehicle interaction,” *2020 4th CAA International Conference on Vehicular Control and Intelligence, CVCi 2020*, pp. 204–209, 12 2020.
- [35] F. Giuliari, I. Hasan, M. Cristani, and F. Galasso, “Transformer networks for trajectory forecasting,” in *2020 25th international conference on pattern recognition (ICPR)*. IEEE, 2021, pp. 10 335–10 342.
- [36] W. Chen, F. Wang, and H. Sun, “S2tnet: Spatio-temporal transformer networks for trajectory prediction in autonomous driving,” in *Asian Conference on Machine Learning*. PMLR, 2021, pp. 454–469.

- [37] A. Bhattacharyya, D. O. Reino, M. Fritz, and B. Schiele, “Euro-pvi: Pedestrian vehicle interactions in dense urban centers,” *2021 IEEE/CVF Conference on Computer Vision and Pattern Recognition (CVPR)*, pp. 6404–6413, 2021.
- [38] J. Tang, J. Sun, C. Wang, and Z. Yang, “Social influence analysis in large-scale networks,” in *Proceedings of the 15th ACM SIGKDD International Conference on Knowledge Discovery and Data Mining*, ser. KDD ’09. New York, NY, USA: Association for Computing Machinery, 2009, p. 807–816. [Online]. Available: <https://doi.org/10.1145/1557019.1557108>
- [39] B. Rozemberczki, C. Allen, and R. Sarkar, “Multi-scale attributed node embedding,” *Journal of Complex Networks*, vol. 9, no. 2, p. cnab014, 2021.
- [40] L. Müller, M. Galkin, C. Morris, and L. Rampásek, “Attending to graph transformers,” *arXiv preprint arXiv:2302.04181*, 2023.
- [41] O. Ronneberger, P. Fischer, and T. Brox, “U-net: Convolutional networks for biomedical image segmentation,” in *Medical Image Computing and Computer-Assisted Intervention–MICCAI 2015: 18th International Conference, Munich, Germany, October 5-9, 2015, Proceedings, Part III 18*. Springer, 2015, pp. 234–241.
- [42] A. Vaswani, N. Shazeer, N. Parmar, J. Uszkoreit, L. Jones, A. N. Gomez, L. u. Kaiser, and I. Polosukhin, “Attention is all you need,” in *Advances in Neural Information Processing Systems*, I. Guyon, U. V. Luxburg, S. Bengio, H. Wallach, R. Fergus, S. Vishwanathan, and R. Garnett, Eds., vol. 30. Curran Associates, Inc., 2017. [Online]. Available: [https://proceedings.neurips.cc/paper\\_files/paper/2017/file/3f5ee243547dee91fbd053c1c4a845aa-Paper.pdf](https://proceedings.neurips.cc/paper_files/paper/2017/file/3f5ee243547dee91fbd053c1c4a845aa-Paper.pdf)
- [43] V. P. Dwivedi, A. T. Luu, T. Laurent, Y. Bengio, and X. Bresson, “Graph neural networks with learnable structural and positional representations,” *arXiv preprint arXiv:2110.07875*, 2021.
- [44] A. Vemula, K. Muelling, and J. Oh, “Social attention: Modeling attention in human crowds,” in *2018 IEEE international Conference on Robotics and Automation (ICRA)*. IEEE, 2018, pp. 4601–4607.
- [45] A. Gupta, J. Johnson, L. Fei-Fei, S. Savarese, and A. Alahi, “Social gan: Socially acceptable trajectories with generative adversarial networks,” in *Proceedings of the IEEE conference on computer vision and pattern recognition*, 2018, pp. 2255–2264.
- [46] C. Wang, Y. Wang, M. Xu, and D. J. Crandall, “Stepwise goal-driven networks for trajectory prediction,” *IEEE Robotics and Automation Letters*, vol. 7, no. 2, pp. 2716–2723, 2022.
- [47] Y. Hu, S. Chen, Y. Zhang, and X. Gu, “Collaborative motion prediction via neural motion message passing,” in *Proceedings of the IEEE/CVF conference on computer vision and pattern recognition*, 2020, pp. 6319–6328.
- [48] C. Yu, X. Ma, J. Ren, H. Zhao, and S. Yi, “Spatio-temporal graph transformer networks for pedestrian trajectory prediction,” in *Computer Vision–ECCV 2020: 16th European Conference, Glasgow, UK, August 23–28, 2020, Proceedings, Part XII 16*. Springer, 2020, pp. 507–523.
- [49] K. Mangalam, H. Girase, S. Agarwal, K.-H. Lee, E. Adeli, J. Malik, and A. Gaidon, “It is not the journey but the destination: Endpoint conditioned trajectory prediction,” in *Computer Vision–ECCV 2020: 16th European Conference, Glasgow, UK, August 23–28, 2020, Proceedings, Part II 16*. Springer, 2020, pp. 759–776.
- [50] C. Xu, M. Li, Z. Ni, Y. Zhang, and S. Chen, “Groupnet: Multiscale hypergraph neural networks for trajectory prediction with relational reasoning,” in *Proceedings of the IEEE/CVF Conference on Computer Vision and Pattern Recognition (CVPR)*, June 2022, pp. 6498–6507.
- [51] T. Gu, G. Chen, J. Li, C. Lin, Y. Rao, J. Zhou, and J. Lu, “Stochastic trajectory prediction via motion indeterminacy diffusion,” in *Proceedings of the IEEE/CVF Conference on Computer Vision and Pattern Recognition (CVPR)*, June 2022, pp. 17 113–17 122.
- [52] Y. Yao, M. Xu, C. Choi, D. J. Crandall, E. M. Atkins, and B. Dariush, “Egocentric vision-based future vehicle localization for intelligent driving assistance systems,” in *2019 International Conference on Robotics and Automation (ICRA)*. IEEE, 2019, pp. 9711–9717.
- [53] T. Yagi, K. Mangalam, R. Yonetani, and Y. Sato, “Future person localization in first-person videos,” 2018.

- [54] A. Bhattacharyya, M. Fritz, and B. Schiele, “Long-term on-board prediction of people in traffic scenes under uncertainty,” 2018.
- [55] A. Rasouli, M. Rohani, and J. Luo, “Pedestrian behavior prediction via multitask learning and categorical interaction modeling,” *CoRR*, vol. abs/2012.03298, 2020. [Online]. Available: <https://arxiv.org/abs/2012.03298>
- [56] D. P. Kingma and M. Welling, “Auto-encoding variational bayes,” *arXiv preprint arXiv:1312.6114*, 2013.
- [57] S. Zamboni, Z. T. Kefato, S. Girdzijauskas, C. Norén, and L. Dal Col, “Pedestrian trajectory prediction with convolutional neural networks,” *Pattern Recognition*, vol. 121, p. 108252, 2022.
- [58] A. Mohamed, K. Qian, M. Elhoseiny, and C. Claudel, “Social-stgcnn: A social spatio-temporal graph convolutional neural network for human trajectory prediction,” in *Proceedings of the IEEE/CVF conference on computer vision and pattern recognition*, 2020, pp. 14 424–14 432.
- [59] C. Yu, X. Ma, J. Ren, H. Zhao, and S. Yi, “Spatio-temporal graph transformer networks for pedestrian trajectory prediction,” in *Computer Vision–ECCV 2020: 16th European Conference, Glasgow, UK, August 23–28, 2020, Proceedings, Part XII 16*. Springer, 2020, pp. 507–523.
- [60] K. Vinogradova, A. Dibrov, and G. Myers, “Towards interpretable semantic segmentation via gradient-weighted class activation mapping (student abstract),” *Proceedings of the AAAI*, vol. 34, no. 10, p. 13943–13944, Apr. 2020. [Online]. Available: <http://dx.doi.org/10.1609/aaai.v34i10.7244>
- [61] R. R. Selvaraju, M. Cogswell, A. Das, R. Vedantam, D. Parikh, and D. Batra, “Grad-cam: Visual explanations from deep networks via gradient-based localization,” in *Proceedings of the IEEE international conference on computer vision*, 2017, pp. 618–626.

## A Conditional Variational Auto-Encoder Preliminaries

ASTRA employs a Conditional Variational Autoencoder (CVAE) [56] framework to address the inherent stochasticity of the prediction task, enabling the generation of  $K$  distinct trajectories for each agent under consideration. Throughout the training phase, it aims to approximate the latent distribution  $Z$  by deducing its mean and variance by utilising Multilayer Perceptrons (MLPs). Subsequently, by employing the divergence loss function (second term in Equation 14), the model pushes the learned distribution  $p_\theta(z_p|x)$ , parameterized by  $\theta$ , to be as close as possible to the ground truth distribution  $q_\Phi(z_q|x, y)$ , parameterized by  $\Phi$ . We use the reparameterization trick to present  $z_p$  and  $z_q$  through the mean and variance pairs of  $(\mu_{z_p}, \sigma_{z_p})$  and  $(\mu_{z_q}, \sigma_{z_q})$ , respectively. After training,  $K$  samples are drawn from the  $Z$  distribution and decoded to form the final trajectories.

## B Loss Function Formulation

The loss for multi-modal trajectories is given in equations equation 13 and equation 14.  $L_{\text{weighted}}(\mathcal{Y}_k, \mathbf{Y})$  is calculated similar to Equation 15.

$$L_{\text{weighted}}(\hat{\mathbf{Y}}, \mathbf{Y}) = \min_{k=1, \dots, K} L_{\text{weighted}}(\mathcal{Y}_k, \mathbf{Y}) \quad (13)$$

$$\mathcal{L}_{\text{final}} = L_{\text{weighted}}(\hat{\mathbf{Y}}, \mathbf{Y}) + D_{KL}(\mathcal{N}(\mu_{z_q}, \sigma_{z_q}) \parallel \mathcal{N}(\mu_{z_p}, \sigma_{z_p})) \quad (14)$$

For deterministic predictions, the final loss is the same as the weighted loss:

$$\mathcal{L}_{\text{final}} = L_{\text{weighted}}(\hat{\mathbf{Y}}, \mathbf{Y}) = \sum_{t=1}^{T_{\text{pred}}} w(t) \cdot L(\hat{Y}_t, Y_t), \quad (15)$$

where  $w(t)$  represent the weighted penalty function (section C) and  $L(\hat{Y}_t, Y_t)$  is the predefined loss function: MSE or Smooth L1 loss (discussed below).

**Mean square error (MSE)**

$$\text{MSE} = \frac{1}{N} \sum_{i=1}^N (y_i - \hat{y}_i)^2 \quad (16)$$

where  $y_i$  and  $\hat{y}_i$  represent, the actual and predicted coordinates, respectively. MSE penalises larger trajectory prediction errors more heavily, ensuring model accuracy in critical scenarios.

**Smooth L1 loss (SL1)**

$$\text{SL1}(y_i, \hat{y}_i) = \begin{cases} 0.5 \times (y_i - \hat{y}_i)^2 & \text{if } |y_i - \hat{y}_i| < 1 \\ |y_i - \hat{y}_i| - 0.5 & \text{otherwise.} \end{cases} \quad (17)$$

Unlike MSE, SL1 effectively balances the treatment of small and large errors. This loss is also less sensitive to outliers, due to its combination of L1 and L2 loss properties.

## C Weighted Penalty Functions

In trajectory prediction, particularly for dynamic entities like pedestrians, vehicles, or other agents, the accuracy of predictions is paramount. The inherent challenge lies in managing the variability and uncertainty that escalates with longer prediction horizons. To address this, we implement different penalization strategies that adjust the model’s emphasis to enhance reliability over extended prediction horizons. Our ablation focuses on three distinct penalty strategies: Linear, Quadratic, and Parabolic. Table 6 presents a quantitative analysis comparing the three penalty strategies as applied to the ETH-UCY (UNIV) dataset using SL1 loss. It can be observed that the Parabolic penalty gives better results compared to other penalization strategies. Figure 9 compares the three weighted penalty strategies for a prediction window of 12 frames. Subsequent sections provide a detailed explanation for each of the penalty strategies.



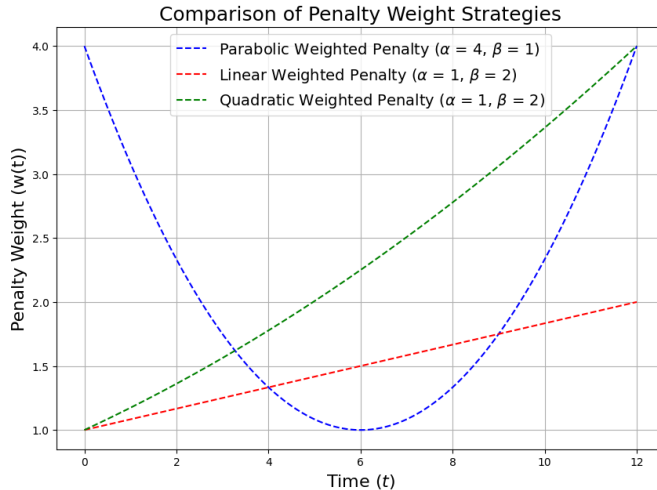


Figure 9: Comparison of various weighted penalty strategies

### C.1 Linear Weighted Penalty

The Linear Weighted Penalty employs a weight function,  $w(t)$ , that linearly increases from a start weight ( $\alpha$ ) to an end weight ( $\beta$ ), over the prediction period. This approach aims to progressively increase the penalty for prediction inaccuracies, particularly toward the latter part of the prediction horizon.

The weight function  $w(t)$  is defined as:

$$w(t) = \alpha + \frac{t}{T_{pred}} \cdot (\beta - \alpha), \quad (18)$$

where  $\alpha$  and  $\beta$  are the weights assigned to the initial and final predicted time steps, respectively.

### C.2 Quadratic Weighted Penalty

The quadratic weighted penalty strategy intensifies the penalty in a quadratic manner as the difference between the prediction time and the past frames increases. This approach is more aggressive than the linear strategy, applying an exponentially increasing weight to errors in later prediction frames. The weight function  $w(t)$  in this case is defined as:

$$w(t) = \left( \alpha + \frac{t}{T_{pred}} \cdot (\beta - \alpha) \right)^2 \quad (19)$$

### C.3 Parabolic Weighted Penalty

The Parabolic Weighted Penalty assigns the maximum weight,  $\alpha$ , to both the initial and final predicted time steps, highlighting their significance. Meanwhile, the minimum weight,  $\beta$  ( $\beta < \alpha$ ), is allocated to the midpoint of the prediction interval. This distribution forms a parabolic trajectory (shown in Figure 9) of weights across the prediction period, as defined by:

$$w(t) = (\alpha - \beta) \cdot \left( 2 \cdot \frac{t}{T_{pred}} - 1 \right)^2 + \beta, \quad (20)$$

Table 6: **Ablation:** Comparing penalization strategies with SL1 loss on ETH-UCY (UNIV) dataset using ASTRA’s SOTA configuration

Loss	minADE <sub>20</sub> /minFDE <sub>20</sub>
<b>Unpenalised</b>	0.37/0.52
<b>Linear</b>	0.33/0.47
<b>Quadratic</b>	0.30/0.46
<b>Parabolic</b>	<b>0.28/0.41</b>



(a) Univ (No Penalty)



(b) Univ (Penalty)



(c) Zara01 (No Penalty)



(d) Zara01 (Penalty)

Figure 10: Qualitative comparison of unpenalised vs. penalised trajectories on ETH-UCY dataset in stochastic setting.



(a) Univ (No Penalty)



(b) Univ (Penalty)



(c) Zara01 (No Penalty)



(d) Zara01 (Penalty)

Figure 11: Qualitative comparison of unpenalised vs. penalised trajectories on ETH-UCY dataset in stochastic setting.

## C.4 Augmentation

To enhance the robustness and generalization of our trajectory prediction model, we implement a data augmentation strategy. This strategy randomly applies rotation and translation transformations to the trajectory sequences [57]. By applying random rotations and translations, our model is trained to be orientation-agnostic and adept at handling positional shifts in agents. These augmentations effectively increase the diversity of the training data, enabling the model to learn more generalized representations of agent movements. This, in turn, enhances the model’s predictive accuracy and robustness, particularly in complex and unpredictable scenarios where pedestrian trajectories can vary significantly due to factors like group dynamics, obstacles, and varying crowd densities.

## D Evaluation Metrics

**ETH-UCY.** To evaluate our model on ETH-UCY, we used commonly employed evaluation metrics [5, 58, 7, 59]: ADE/FDE and minADE<sub>K</sub>/minFDE<sub>K</sub>. Average Displacement Error (ADE) computes the average Euclidean distance between the predicted trajectory and the true trajectory across all prediction time steps for each agent. minADE<sub>K</sub> refers to the minimum ADE out of K randomly generated trajectories and ground truth future trajectories. We also used the Final Displacement Error (FDE), which focuses on the prediction accuracy at the final time step. It computes the Euclidean distance between the predicted and actual positions of each agent at the last prediction time step. minFDE<sub>K</sub> refers to the minimum FDE out of K randomly generated trajectories and ground truth future trajectories. For multimodal trajectory prediction, minADE<sub>K</sub> and minFDE<sub>K</sub> metrics are used for evaluation.

$$\text{ADE} = \frac{1}{T_{pred}} \sum_{t=1}^{T_{pred}} \|Y_t^a - \hat{Y}_t^a\|_2. \quad (21)$$

$$\text{minADE}_K = \min_k \left( \frac{1}{T_{pred}} \sum_{t=1}^{T_{pred}} \|Y_t^a - \hat{Y}_{t,k}^a\|_2 \right) \quad (22)$$

$$\text{FDE} = \|Y_{T_{pred}}^a - \hat{Y}_{T_{pred}}^a\|_2 \quad (23)$$

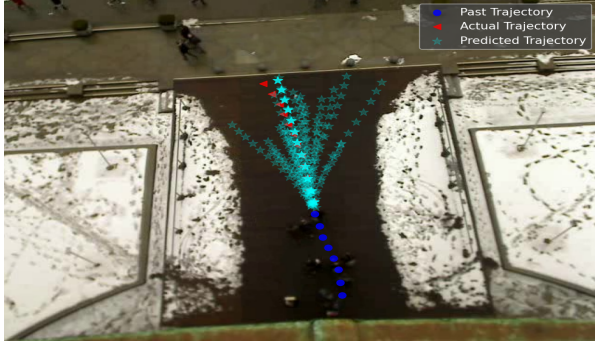
$$\text{minFDE}_K = \min_k \left( \|Y_{T_{pred}}^a - \hat{Y}_{T_{pred},k}^a\|_2 \right) \quad (24)$$

**PIE.** For the PIE Dataset, the ADE and FDE metrics are calculated based on the centroid of the bounding box [17, 2], denoted as Centre average displacement error for the bounding box (CADE) and Centre final displacement error for the bounding box (CFDE). In addition, we reported the average and final Root Mean Square Error (RMSE) of bounding box coordinates, denoted as ARB and FRB, respectively [10].

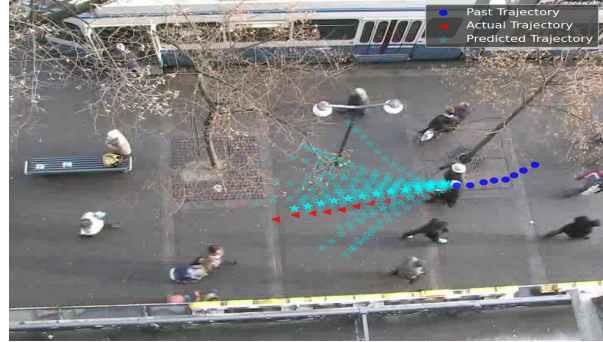
## E Grad-CAM visualizations

Grad-CAM images were obtained by generating heatmaps overlaid onto the original image to aid in validating the relevance of highlighted regions. To obtain the Grad-CAM visualization, a single-channel output segmentation map was obtained from the pre-trained U-Net network, representing the probability of each pixel location being a keypoint [13]. Probabilities were aggregated across all pixels, by comparing them with true keypoints and gradients of activation for the initial layer were extracted, similar to the approach taken by [60]. Utilizing these gradients, a weighted average of the activation maps of the initial layer was computed to reconstruct the heatmap, similar to the method described in [61], for the Grad-CAM visualization. Overlaying this heatmap onto the original image highlights the regions that contribute significantly to the keypoint predictions made by the model.

To ease reading the paper, Table 7 and 8 list the abbreviations and the mathematical symbols mentioned in the paper, respectively.



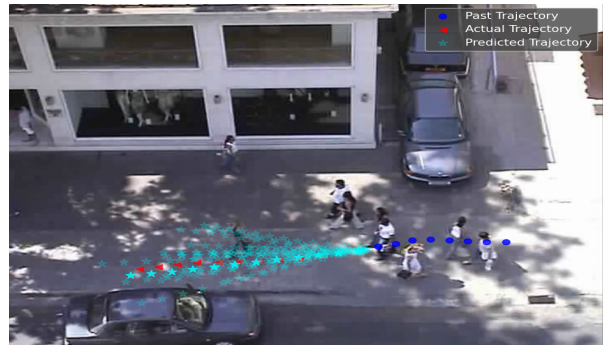
(a) ETH



(b) Hotel



(c) Univ



(d) Zara1

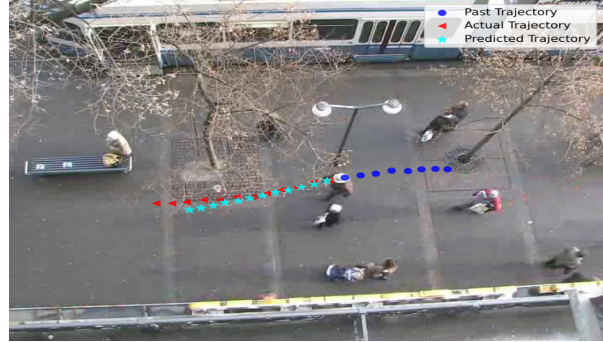


(e) Zara2

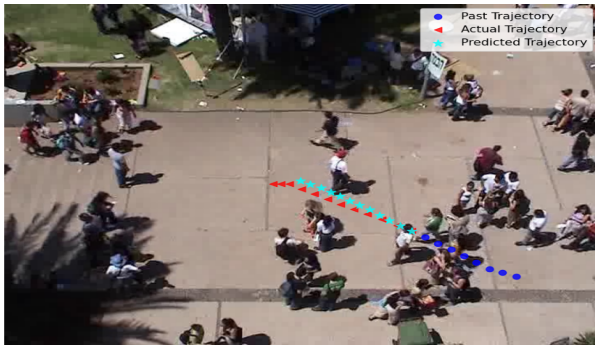
Figure 12: Multi-modal trajectory visualizations on ETH-UCY dataset (BEV)



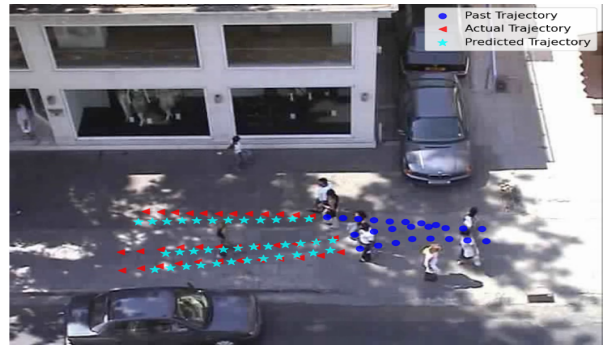
(a) ETH



(b) Hotel



(c) Univ



(d) Zara1



(e) Zara2

Figure 13: Deterministic trajectory visualizations on ETH-UCY dataset (BEV)

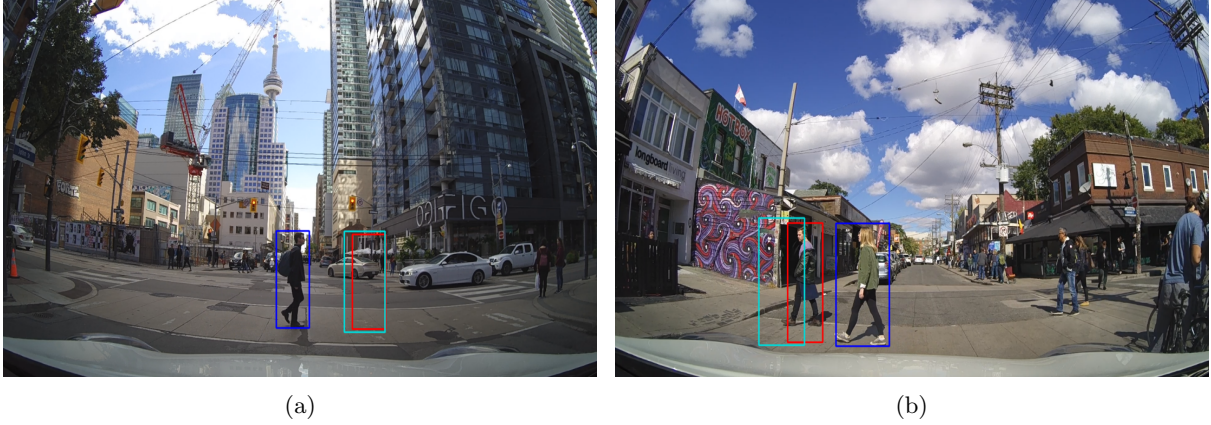


Figure 14: Trajectory Visualizations on PIE Dataset (EVV) where the red and cyan bounding box indicates the ground-truth and predicted final position respectively and the blue bounding box indicates the start position.

Table 7: Table of Abbreviations Used

Abbreviation/Term	Description
ASTRA	Agent-Scene aware model for pedestrian trajectory forecasting
BEV	Bird's Eye View
EVV	Ego-Vehicle View
AV	Autonomous Vehicle
MLP	Multi-Layer Perceptron
CVAE	Conditional Variational Auto-Encoder
GNN	Graph Neural Network
RWPE	Random Walk Positional Encoding
MSE	Mean Square Error (Loss Function)
SL1	Smooth L1 Loss (Loss Function)
ADE	Average Displacement Error
FDE	Final Displacement Error
CADE	Centre average displacement error for the bounding box
CFDE	Centre final displacement error for the bounding box
ARB	Average Root Mean Square Error for the bounding box
FRB	Final Root Mean Square Error for the bounding box

Table 8: Table of Mathematical Symbols Used

<b>Symbols</b>	<b>Description</b>
$N$	Total number of predictions in MSE calculation
$\mathbf{X}$	Observed trajectories of agents
$\mathbf{Y}$	Groundtruth future trajectories of agents
$\hat{\mathbf{Y}}$	Predicted trajectories of agents
$T_{\text{obs}}$	Number of past time instants for observation
$T_{\text{pred}}$	Number of future time instants for prediction
$\mathbf{I}_{t=1:T_{\text{Obs}}}$	Sequence of past input frame images
$X_t^a$	Observed coordinates for agent $a$ at time $t$
$\hat{Y}_t^a$	Predicted coordinates for agent $a$ at time $t$
$A$	Number of target agents
$e_{ij}$	Edge weight in graph $G$ between nodes $i$ and $j$
$d(v_i, v_j)$	Distance between agents $v_i$ and $v_j$
$w(t)$	Weight function in weighted-penalty strategy
$w_{\text{start}}$	Start weight in weighted-penalty strategy
$w_{\text{end}}$	End weight in weighted-penalty strategy
$\Psi_{\text{Scene}}$	Latent representation of scene(past frame) obtained from U-Net encoder
$\Phi_{\text{Scene}}$	Scene-aware embeddings
$\mathbf{T}_{\text{Scene-aware}}$	Scene-aware Transformer encoder
$\Upsilon_{\text{Encoder}}$	U-Net Encoder
$\Gamma_{\text{Scene}}$	Multi-layer Perceptron layer for Scene embeddings
$\Phi_{\text{Temporal}}$	Temporal encoding
$\Gamma_{\text{Spatial}}$	Multi-layer Perceptron layer for Spatial embeddings
$\Phi_{\text{Spatial}}$	Spatial embeddings
$\Gamma_{\text{Social}}$	Multi-layer Perceptron layer for Social embeddings
$\Phi_{\text{Social}}$	Social Embeddings
$\mathbf{T}_{\text{Agent-aware}}$	Agent-aware Transformer encoder
$\Phi_{\text{Agents}}$	Agent-aware embeddings
$L_{\text{weighted}}(\hat{Y}, Y)$	Weighted-penalty Loss Function